Numerical modelling of Cenozoic stress patterns in the Mid Norwegian Margin and the northern Sea

Pascal, C.; Gabrielsen, R.H.

published in
Tectonics
2001

DOI (link to publisher)
10.1029/2001TC900007

document version
Publisher's PDF, also known as Version of record

TECTONICS, VOL. 20, NO. 4, PAGES 585-599, AUGUST 2001

Numerical modeling of Cenozoic stress patterns in the mid-Norwegian margin and the northern North Sea

Christophe Pascal[1] and Roy H. Gabrielsen

Geological Institute, University of Bergen, Bergen, Norway

Abstract. Numerical modeling of Cenozoic stress patterns in the northern North Sea and the mid-Norwegian margin is presented, and the sense of potential slip along major fault planes belonging to the two areas is restored. We assume that the main regional source of stresses is the Atlantic ridge push as demonstrated by previous studies. Furthermore, we also assume a nearly consistent NW-SE strike for the far-field stress from continental breakup between Greenland and Norway (earliest Eocene) to present day. First, we applied the commercial two-dimensional distinct element method (UDEC) to simulate Cenozoic stress and displacement patterns in the study area. Variations in rheology and major fault zones were introduced into the model. The Møre-Trøndelag Fault Complex and its inferred continuation into the Shetland Platform forms the major mechanical discontinuity in the model. Second, we used the SORTAN method, developed at the University of Paris VI, to predict the sense of potential slip along major fault planes. The input for the SORTAN model was constrained by the geometry of the selected fault planes and local principal stress directions extracted from the UDEC modeling. Our results show that the Møre-Trøndelag Fault Complex and its inferred continuation into the Shetland Platform act as a weak fault zone. This fault zone divides the study area into two different stress provinces: the continental margin and the northern North Sea. This result agrees well with the observed differences in Cenozoic structural evolution of the two areas. Compressive structures are observed along the continental margin, whereas relative tectonic quiescence characterizes the northern North Sea during the Tertiary. The restored stress patterns in the northern North Sea and the mid-Norwegian margin also agree well with the observed present-day stress configuration. Our analysis demonstrates a method to reconstruct the sense of slip on major fault planes by combining two complementary numerical tools (UDEC and SORTAN). As a result, it is demonstrated that oblique-slip motions are mainly expected, in particular, strike-slip and reverse dip-slip faulting are simulated.

1. Introduction

Comparison of the Tertiary to present-day structural evolution of the mid-Norwegian margin (i.e., Møre and Vøring Basins) with that of the northern North Sea reveals that both areas have been dominated by subsidence [*Ziegler*, 1990; *Jordt et al.*, 1995]. However, the mid-Norwegian margin has been subject to mild shortening since continental breakup took place in the Norwegian Sea in the earliest Eocene. Thus Cenozoic compressive structures, such as arches, synclines and anticlines, and inverted normal faults, have been mapped in the mid-Norwegian margin [*Blystad et al.*, 1995; *Doré and Lundin*, 1996; *Doré et al.*, 1997; *Vågnes et al.*, 1998], whereas no evidence of major Cenozoic inversion exists in the Viking Graben and the Sogn Graben of the northern North Sea basin. The mid-Norwegian margin and the northern North Sea are separated by the Møre-Trøndelag Fault Complex (Figure 1), a structure that is believed to provide distinct stress fields in the areas to its north and the areas to its south since Permian times [*Gabrielsen et al.*, 1999]. Similar Cenozoic inversion structures are common on the Faeroe Plateau [*Boldreel and Andersen*, 1998]. The timing and the location of the contractional structures in these areas favors ridge push as the main source of the compression [*Vågnes et al.*, 1998], although the potential influence from plate reorganization [*Doré and Lundin*, 1996; *Doré et al.*, 1997] and the alpine collision should not be overlooked.

In order to model strain and stress patterns inside the two areas we used the two-dimensional UDEC software [*Cundall*, 1980]. Considering the size of the study area and hence the amount of data involved, a 2-D "thin plate" model was selected for the present modeling. Particular attention was paid in modeling the larger Møre-Trøndelag Fault Complex, which was treated as the major zone of weakness in the study area. This approach permits (1) checking the role of the zone of weakness in separating the northern North Sea from the mid-Norwegian margin and (2) restoring the stress patterns affecting the two areas. Finally, numerical output from UDEC (i.e., strike of principal axes of stress) was used as input in analysis by the SORTAN method. This method allows reconstruction of senses of potential slip along major fault planes belonging to the study area.

2. Geological Setting

The study area is influenced by several structural boundary zones, which are potentially of great importance for stress transfer and stress perturbations, as it has been shown by the numerical study from *Gölke et al.* [1996]. Among them we find the continent-ocean boundary, the transition from the extended margin to the thick continental crust onshore Norway, and some first-order fault complexes (Figure 1). All these structures are clearly visible in potential field data covering the study area (e.g., Figure 2).

[1]Now at Faculty of Earth Sciences, Vrije Universiteit, Amsterdam, Netherlands.

Paper number 2001TC900007.
0278-7407/01/2001TC900007$12.00

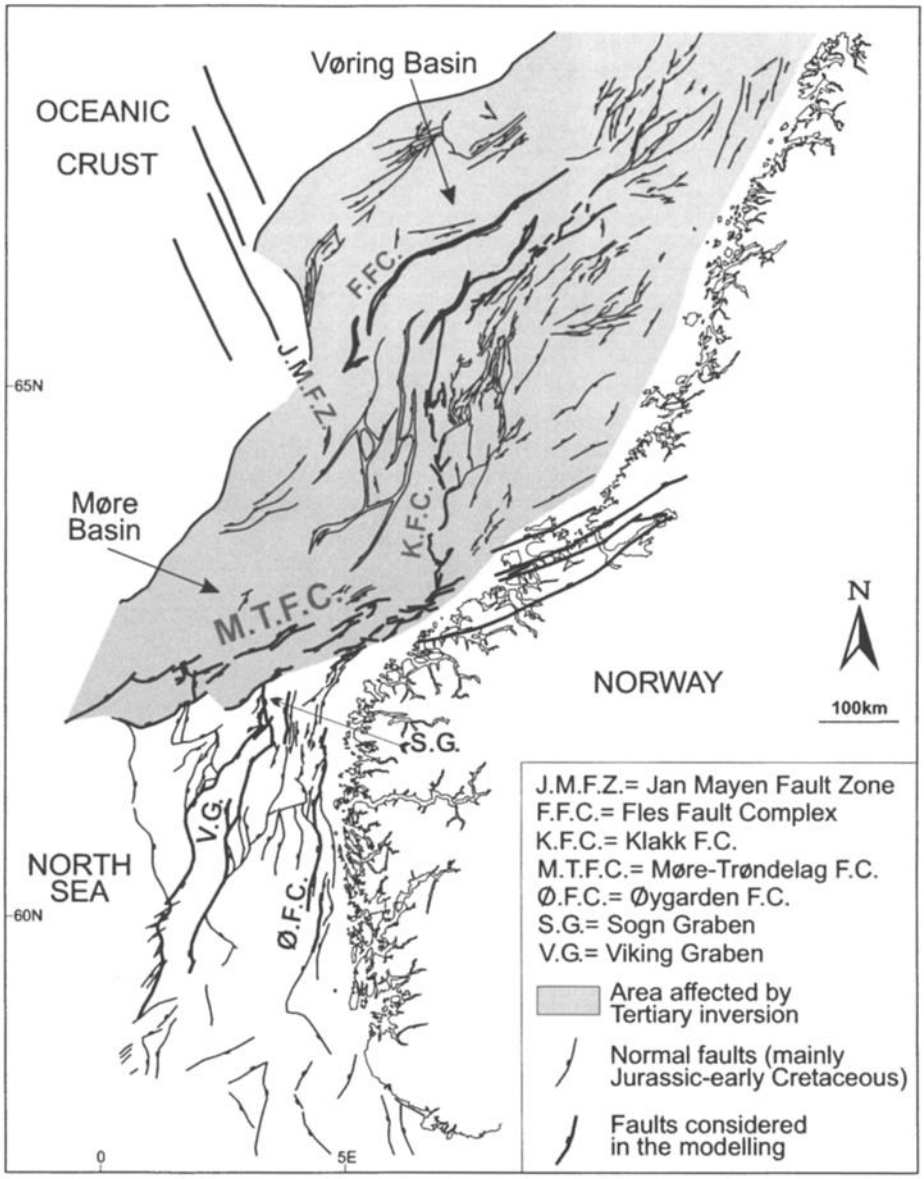

Figure 1. Simplified structural map of the mid-Norwegian margin and the northern North Sea.

The continent-ocean boundary is characterized by a complex structure and a partly serrated geometry. The complexity and its profound nature are mirrored in contrasting spreading configurations. Spreading north of the Jan Mayen Fracture Zone is symmetric, whereas spreading south of the Jan Mayen was influenced by a systematic westward drift of the spreading axis [*Eldholm et al.*, 1990]. Generally, considerable structural and velocity field anisotropy exists along the continent-ocean boundary [*Midzi et al.*, 1999]. The NNW trending Jan Mayen Fracture Zone [*Sykes*, 1965; *Talwani and Eldholm*, 1972, 1977] has probably imposed some control on the structuring of the mid-Norwegian margin. The westernmost segment of this structure includes the presently active transform, which separates the spreading Mohns Ridge in the north from the Kolbeinsey Ridge in the south. Lineaments parallel to the Jan Mayen Fracture Zone are seen to crosscut the Møre Trøndelag Fault Complex onshore [*Gabrielsen and Ramberg*, 1979; *Aanstad et al.*, 1981].

The Møre-Trøndelag Fault Complex is one of the most prominent fault zones of Norway, onshore and offshore [*Oftedahl*, 1972, 1975; *Gabrielsen and Ramberg*, 1979; *Gabrielsen et al.*, 1984, 1999; *Price and Rattey*, 1984; *Doré and Gage*, 1987; *Grønlie and Roberts*, 1989; *Blystad et al.*, 1995]. It strikes ENE-WSW, paralleling the coastline of south central Norway, and separates the northern North Sea basin system from the deep Cretaceous Møre and Vøring Basins (Figure 1). Deep reflection seismic data suggest that it is a steeply dipping crustal-scale fault [*Hurich*, 1996]. It coincides with a positive gravity anomaly that can be followed across the northernmost North Sea to the East Shetland Platform (Figure 2). The Møre-Trøndelag Fault Complex was an important feature during the Caledonian orogeny [*Torsvik et*

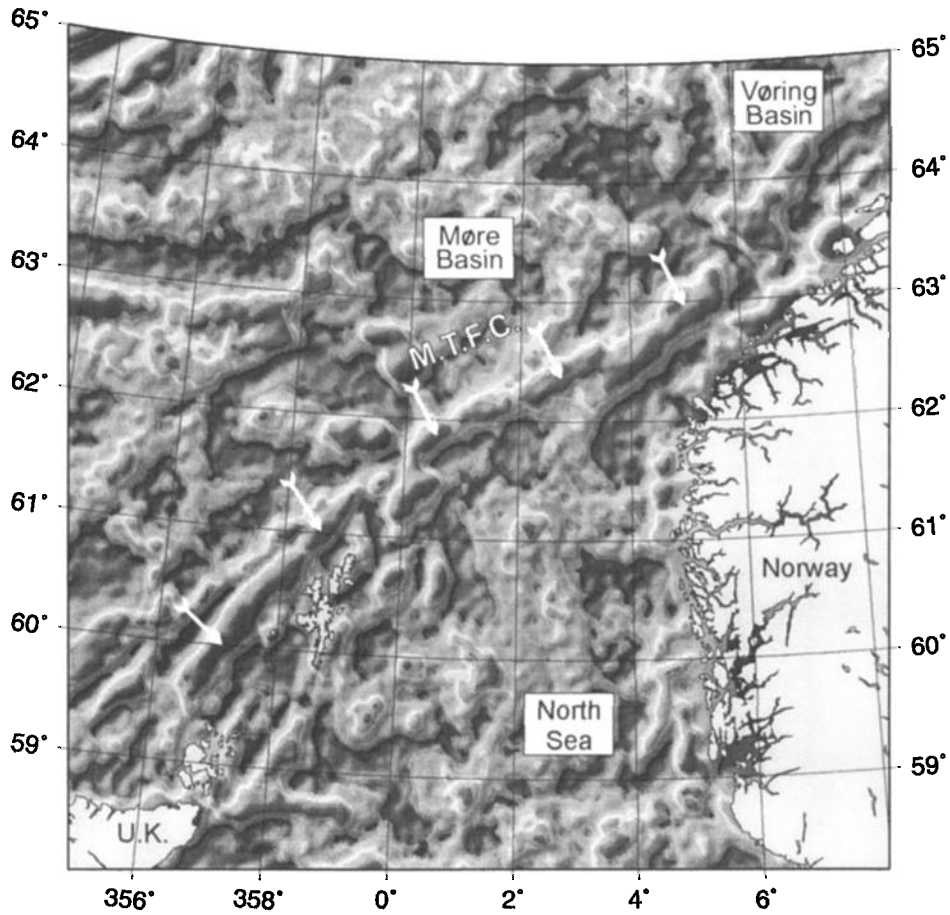

Figure 2. Free-air gravimetry anomalies (240 km high-pass filter) in the Scottish and the mid-Norwegian continental margins and in the northern North Sea. Note the well-pronounced positive anomaly (white arrows) corresponding to the basement highs involved into the Møre-Trøndelag Fault Complex and into its likely continuation north of Scotland. Data from ERS 1 and Geosat are after *Sandwell and Smith* [1997].

al., 1989] and probably affected the outline of the late Caledonian collapse as well [*Séranne*, 1992]. The fault complex has been repeatedly reactivated from the late Palaeozoic through the Mesozoic and Cenozoic [*Grønlie and Roberts*, 1989; *Grønlie et al.*, 1990; *Gabrielsen et al.*, 1999], and seismological observations suggest that the zone is still active [*Gabrielsen*, 1989; *Bungum et al.*, 1991].

The area to the north of the Møre Trøndelag Fault Complex comprises the Trøndelag Platform and the Cretaceous Møre and Vøring Basins. The platform is separated from the basins by the Klakk Fault Complex, striking N-S in the south, turning to NE-SW in the north. The Fles Fault Complex is another prominent structure, which runs parallel to the Klakk Fault Complex in the central part of the Vøring Basin. The formal definitions and descriptions of these structures are given by *Blystad et al.* [1995]. These important zones of weakness have been incorporated in the model to estimate the total horizontal stress pattern and the displacement field of the study area.

3. Numerical Tools

3.1. The 2-D Distinct Element Method (UDEC)

The main principles and the potential of the distinct element method (DEM) is outlined in Appendix A, and a complete mathematical description is provided by *Cundall* [1980] and *Last and Harper* [1990]. UDEC [*Cundall*, 1971, 1980] is a 2-D version of the DEM. The purpose of the numerical DEM is to calculate stress and strain inside discontinuous media such as fractured rock masses. In the DEM the medium is divided into several distinct blocks (Figure 3). Using finite difference techniques, classical continuum constitutive laws are applied for the interior of each block, and relative displacements between blocks are calculated. Blocks interact at their contacts, where constitutive laws are defined. Hence external boundary conditions are introduced for the complete set of blocks, and internal boundary conditions are calculated at each block boundary. Technically speaking, the DEM is based on an explicit calculation procedure, which introduces better numerical stability. Mechanical equations are time-integrated.

3.2. The SORTAN Method

SORTAN is an analytical procedure to calculate the sense of slip induced by stresses along fault planes. The method and software have been developed at University of Paris VI

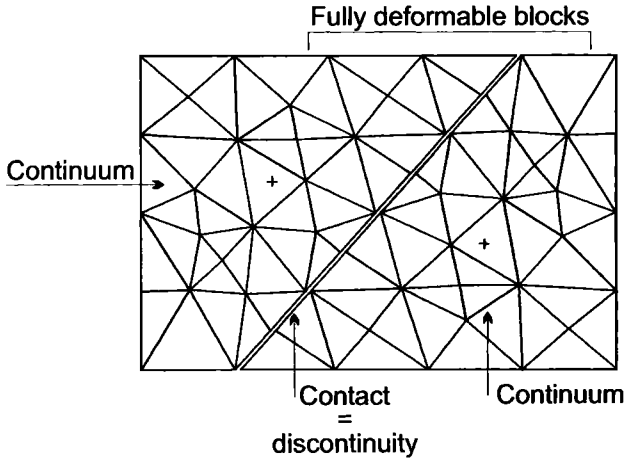

Figure 3. Basic elements of a DEM model. The medium to be modeled is split into distincts blocks. Strain and stresses are calculated at grid points inside each block (continuum medium) by classical finite differences method. Blocks interact through their contacts (discontinuities).

[*Pascal*, 1998; C. Pascal and J. Angelier, Sortan an analytical method to determine fault slip as induced by stresses, submitted to the *Journal of Structural Geology*, 2001]. For simplicity, the method is presented in Appendix B using J. Angelier's formalism [*Angelier*, 1975, 1979].

The method is based on the following "Wallace-Bott" assumptions [*Wallace*, 1951; *Bott*, 1959]: (1) slip on fault surfaces occurs parallel to the applied shear stress, (2) faults are planar, (3) blocks are rigid, (4) neither stress perturbations nor block rotations along fault surfaces occur, and (5) the applied stress state is stable for each tectonic event. Since the sense of shear stress vectors depends only on the orientation of the three principal stress axes and on the geometry of the shape of the stress ellipsoid, stress tensor analysis can be simplified by using a reduced stress tensor technique [*Carey and Brunier*, 1974; *Angelier*, 1975, 1979].

The SORTAN method requires only four input numerical parameters: two parameters to describe the applied stress state (the azimuth θ and the shape ratio Φ (see Appendix B)) and two parameters to describe the geometry of the studied fault plane (the dip direction d and the dip angle p). However, the type of stress regime (e.g., the spatial configuration of the three principal stress axes) to be introduced in the model must be known or assumed before the application.

4. Simulation of Cenozoic Stress Patterns Using UDEC

4.1. Formulation of the Problem

The area considered in the present model (Figures 2 and 4) is located between 5°W and 10°E longitude and between 58° and 68°N latitude. Linear elastic behavior is assumed for the modeled area. Four domains with distinct rheologies were defined: (1) oceanic crust with high Young's modulus (E=100 GPa), (2) sedimentary basins belonging to the continental margin and to the northern North Sea, both areas being less competent (E=30 GPa), (3) a very deformable (E=3 GPa) zone of weakness associated to the Møre-Trøndelag Fault Complex and to its continuation into the West Shetland Platform, and (4) the very competent basement (E=70 GPa) of south Norway. The Young's modulus values selected for each domain were extracted from the literature [e.g., *Carmichael*, 1989]. The empirical choice of the Young's modulus for the zone of weakness will be discussed below [see also *Homberg et al.*, 1997]. We chose for the entire study area an average Poisson's ratio value equal to 0.25.

Only the major discontinuities of the studied area were introduced into the model. These include the Jan Mayen Fault

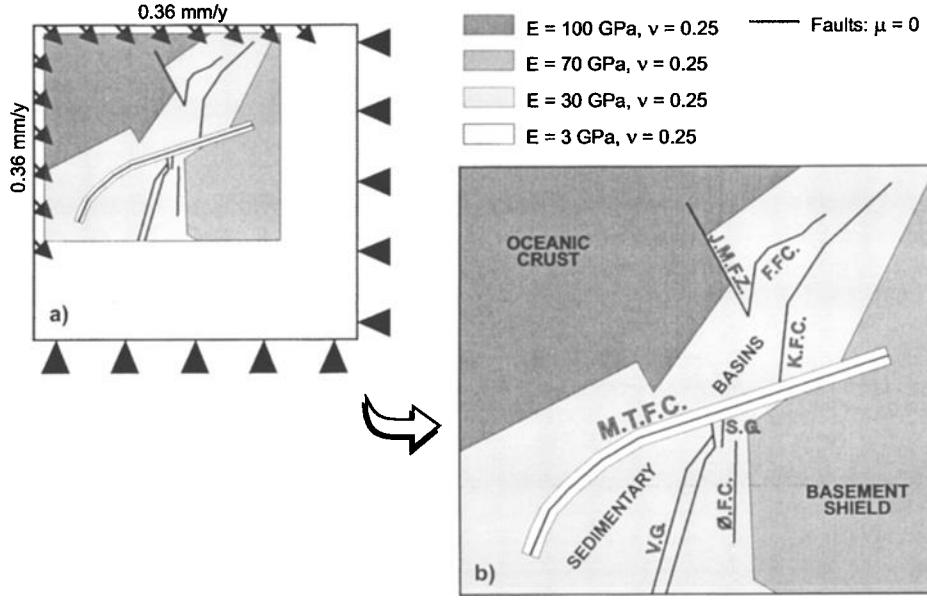

Figure 4. Geometry and mechanical parameters used for the UDEC modeling. See key in Figure 1. E = Young's modulus, ν = Poisson's ratio, μ = faults friction.

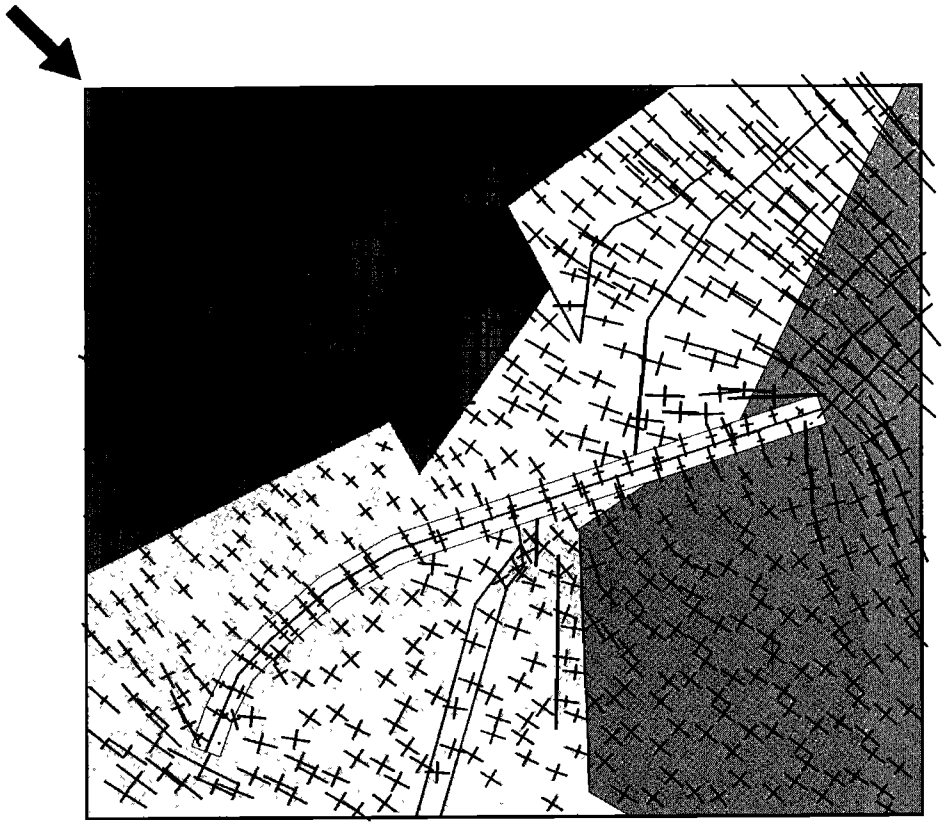

Figure 5. Stress patterns simulated by UDEC.

Complex, the Fles Fault Complex, the Klakk Fault Complex (and its continuation to the NE), the Møre-Trøndelag Fault Complex and its continuation into the West Shetland Platform, the Øygarden Fault Complex, and the Sogn Graben and Viking Graben border faults (Figures 1 and 4). These major fault zones are mainly associated with borders of the sedimentary basins. They were selected because of their Tertiary tectonic importance (e.g., Jan Mayen Fault Complex, Fles Fault Complex, and Møre-Trøndelag Fault Complex) [see *Blystad et al.*, 1995] and because of their present-day seismic activity [*Gabrielsen*, 1989; *Bungum et al.*, 1991; *Byrkjeland et al.*, 2000].

The 2-D model (Figure 4) represents a present-day layer of the brittle upper crust situated at depth between 3 and 4 km. At this depth, all structures that are described in the modeling are encountered. However, the simple 2-D model is not able to simulate the stress magnitudes expected at such depths (i.e., in the range of 100 MPa). Stress magnitudes simulated by the UDEC model range between 0.01 and 0.1 MPa. Thus we are not able to predict stress magnitudes, and the only relevant information to extract from the model results is principal stress axes directions, which is input required for SORTAN.

In order to model eventual displacements and because the modeled stress magnitudes are much too low to trigger displacement along faults with realistic coefficients of friction [e.g., *Byerlee*, 1978], the friction on faults was reduced to zero. Again, no rigorous simulation of the amount of shear displacements is accounted for by the present model. However, we can explore the sensitivity of each fault to be reactivated in the framework of the modeled stress field orientations.

The most important boundary condition introduced to the model was that the present Atlantic ridge push is assumed to have lasted from earliest Eocene (continental breakup) to present day [*Stephansson*, 1988; *Spann et al.*, 1991; *Fejerskov et al.*, 1995]. This assumption is supported by the occurrence in different places along the margin of Eocene to present-day compressive structures identified in seismic reflection lines and whose age is calibrated by wells [*Blystad et al.*, 1995; *Grunnaleite and Gabrielsen*, 1995; *Doré and Lundin*, 1996; *Boldreel and Andersen*, 1998; *Langaker*, 1998; *Vågnes et al.*, 1998]. In addition, crosscutting relationships between microfaults and dated magmatic rocks demonstrate that compression started in the Faeroe Islands in earliest Eocene [*Geoffroy et al.*, 1994]. This implies that we aim to simulate the present-day configuration, assuming that this is also valid for the time span considered. Therefore displacement velocities (0.36 mm of shortening per year, Figure 4) were applied to the western and northern boundaries of the model. The velocity has been calculated according to the estimated total shortening of the mid-Norwegian margin during the considered time span. *Vågnes et al.* [1998] estimated by line balancing 0.5 and 1% of shortening for the Ormen Lange Dome and the Helland-Hansen Arch, respectively. They extrapolated 2-3% of shortening for the whole mid-Norwegian margin. These values are probably underestimated

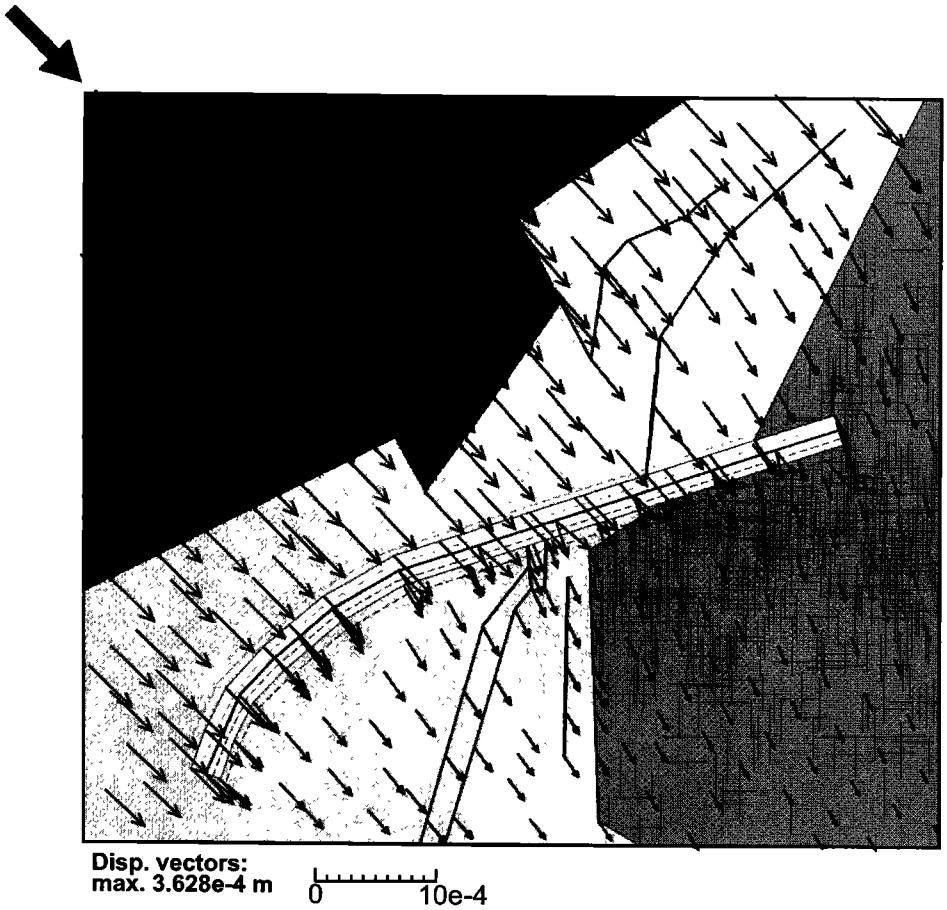

Figure 6. Displacement field simulated by UDEC. The boxed areas B_N and B_S correspond to the locations where numerical output has been extracted from (see Figure 7). The lengths of the arrows are proportional to displacement magnitudes.

because (1) contribution from small-scale structures was not considered and (2) ~10% of the total amount of shortening was probably accommodated by plastic deformation of rocks. In the present study we adopted the value in excess of 5% of shortening for the whole mid-Norwegian margin. As suggested by the constant rate of growth of the Ormen Lange Dome from earliest Eocene to present day [*Vågnes et al.*, 1998], a constant SE trend of the "ridge push" was assumed. The southern and the eastern boundaries of the model were kept fixed. In order to avoid edge effects (stress rotations) these boundaries (Figure 4) were removed from the study area.

4.2. Results of UDEC modeling

4.2.1. Simulated stress patterns. Figure 5 shows the simulated stress pattern. Stress rotations up to 45° occur at boundaries between domains with different rheologies as, for example, at the boundaries between the oceanic crust and the sedimentary basins or between the sedimentary basins and the competent crust of the onshore Scandinavian Shield. Stress rotations become more pronounced where the boundary considered is orientated obliquely to the applied far-field stress, such as the north-south boundary between south Norwegian mainland and the North Sea.

More drastic stress deflections are visible inside (where σ_H becomes perpendicular to the fault line) and nearby the weak zone associated with the Møre-Trøndelag Fault Complex and its continuation. As would be expected, large stress rotations also occur near the tips of the fault zone (where σ_H becomes parallel or perpendicular to the fault line, Figure 5). We note counterclockwise stress rotations north to the eastern tip of the zone of weakness and clockwise stress rotations to its south. This classical stress pattern for strike-slip faults [see *Anderson*, 1951, Figure 35, p. 163] suggests dextral reactivation of this branch of the fault zone. The possible dextral rejuvenation (i.e., strong stress deflections at the eastern tip of the fault) of the Møre-Trøndelag Fault Complex is the only significant reactivation that is suggested by the present UDEC model. Note that reverse faulting is also observed in places along the Møre-Trøndelag Fault Complex [*Blystad et al.*, 1995] but cannot be accounted by our 2-D model.

Maximum principal stresses become perpendicular to the strike of the fault line inside the fault zone (Figure 5). Such a phenomenon is well established for other major transcurrent fault zones (e.g., the San Adreas Fault) [*Zoback et al.*, 1987]. This effect arises in our model from the contrasting rheologies between the fault zone (E=3 GPa) and the surrounding areas

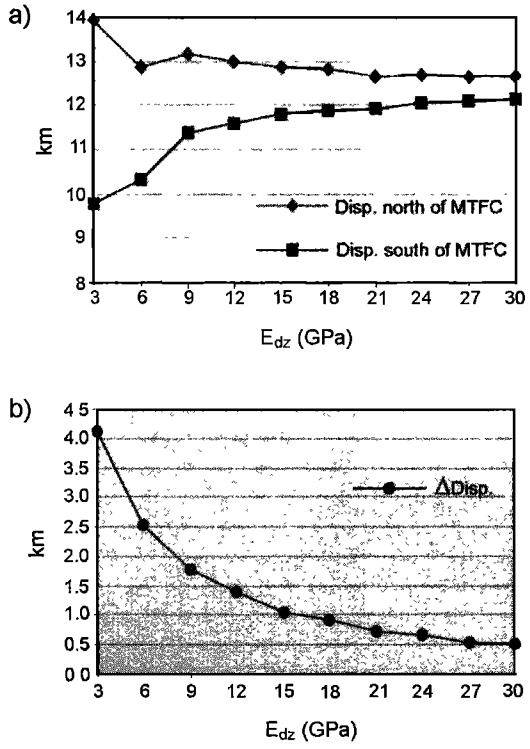

Figure 7. Influence of the Young's modulus of the fault zone E_{dz} on displacement magnitudes north and south of the Møre-Trøndelag Fault Complex. The displacements are extrapolated to the considered time span (55Myr). (a) Averaged displacements north and south of the zone of weakness versus E_{dz}. (b) Differences between displacements calculated north of the zone of weakness and displacements calculated south of the zone of weakness versus E_{dz}.

(30 and 70 GPa). Stress magnitudes are decreased inside the fault zone, as expected owing to the lower "strength" of this zone.

For the northern North Sea the simulated stress pattern (Figure 5) is nearly isotropic in the horizontal plane, with the magnitude of the maximum horizontal principal stress being close to that of the minimum horizontal principal stress. Still, a significant counterclockwise rotation of the stress field is observed as compared to the strike of the applied boundary stresses.

4.2.2 Simulated displacement vectors. The displacement vectors in the model are presented as arrows (Figure 6). No major changes in displacement vectors occur inside the area that is dominated by oceanic crust (Figures 4 and 6). Thus the relatively strong oceanic crust (i.e., E=100 MPa) allows conservation of the applied boundary strain throughout the oceanic domain, and boundary strain is almost totally transferred to the margin. If we consider the entire area covered by the model, an important decrease of displacement magnitudes from NW to SE is noted. This effect is expected as a consequence of the selected boundary conditions (e.g., northern and western boundaries submitted to loading but southern and eastern boundaries kept fixed, Figure 4).

However, it is obvious that calculated displacements suddenly drop across the zone of weakness (Figure 6). This is related to the contrasting rheologies between the fault zone itself and the surrounding areas and happens because part of the strain is focused inside the fault zone, where rocks are less competent. Assuming that the mechanical parameters introduced for areas outside the fault zone are correct, we can therefore concede that the "shield effect" depends only on the rheology of the fault zone. Unfortunately, the rheology of the fault zone is the most unconstrained input parameter in our model, and this parameter needs to be further investigated.

For quantification, displacements north and south of the zone of weakness were compared for different values of the Young's modulus of the fault zone (E_{dz}). In order to avoid the effects of the systematic decrease in displacement magnitudes from NW to SE, as induced by the chosen boundary conditions, displacement values were sampled in small areas located close to the northern and the southern boundaries of the fault zone (boxed areas B_N and B_S in Figure 6).

Averaged displacement values were calculated as a function of E_{dz} for the southern and the northern areas, using the corresponding displacement values (displacement per year), and the averaged displacements from both areas were

Table 1. Fault Geometries (Dip and Dip Direction) and Local Principal Stresses Directions (σ_1 Strikes) Introduced as Input for the SORTAN Modeling[a]

Fault	Dip Direction, deg	Dip, deg	Source	Azimuth σ_1, deg
1	N285	41	*Blystad et al.* [1995]	N135
2	N275	71	*Blystad et al.* [1995]	N120
3	N271	71	*Blystad et al.* [1995]	N120
4	N251	41	*Blystad et al.* [1995]	N102
5	N137	56	*Blystad et al.* [1995]	N160
6	N270	52	*Faeserth* [1996]	N135
7	N289	58	*Kjennerud* [1997]	N110
8	N237	51	*Christiansson et al.* [2000]	N110
9	N279	42	*Christiansson et al.* [2000]	N110
10	N274	76	*Christiansson et al.* [2000]	N110
11	N262	53	*ter Voorde* [1996]	N120
12	N292	54	*Christiansson et al.* [2000]	N120
13	N123	57	*Christiansson et al.* [2000]	N126
14	N098	61	*Huser* [1994]	N126
15	N117	46	*Christiansson et al.* [2000]	N120
16	N283	68	*Christiansson et al.* [2000]	N120
17	N129	30	*Kjennerud* [1997]	N120
18	N073	38	*Faeserth* [1996]	N120
19	N109	20	*Faeserth et al.* [1995]	N120
20	N160	46	*Blystad et al.* [1995]	N160
21	N284	59	*Blystad et al.* [1995]	N115
22	N123	45	*Blystad et al.* [1995]	N119
23	N161	33	*Blystad et al.* [1995]	N130
24	N142	65	*Blystad et al.* [1995]	N135

[a]Fault geometries come from various sources; local principal stresses directions are simulated by UDEC (Figure 5). "Local" refers to locations at or nearby the studied fault planes.

extrapolated to the time span from continental breakup to present day (i.e., 55 Myr). Finally, the averaged displacements, normalized to 55 Myr for both areas (versus E_{dz}), and the difference between the averaged displacements in the northern area and in the southern area (versus E_{dz} and normalised to 55 Myr) were plotted (Figures 7a and 7b). Those plots show that the averaged displacements south to the zone of weakness increase with E_{dz} (Figure 7a). This implies that for a more rigid fault zone, more strain is transmitted across it. On the other hand, we note that the averaged displacements calculated north of the zone of weakness decrease with E_{dz} (Figure 7a), meaning that the more rigid the fault zone is, the less strain is concentrated in the continental margin north of the zone of weakness. Also, if E_{dz} is equal to 30 GPa, which is the Young's modulus value of the surrounding sedimentary basins (Figure 4), the displacements calculated on both sides of the fault zone are almost equal. In giving similar rheological parameters to the fault zone and the surrounding areas, no "shield effect" is detected in connection with the fault zone. The small difference, which is still observed for E_{dz}=30 GPa (Figure 7a), arises from the onshore area of our model, where mechanical contrast still exists between the fault zone (E_{dz}=30 GPa) and the surrounding rocks (E=70 GPa). Finally, the difference in averaged magnitudes of displacements decreases exponentially as a function of E_{dz} (Figure 7b). The differences increase very fast for $E_{dz} < 9$ GPa and become significant (e.g., < 1 km) for $E_{dz} >$ 12 GPa. Clockwise rotation of displacement vectors between the area north of the fault zone and the area to the south (Figure 6) is a function of the shield effect of the fault zone and the applied boundary conditions.

Pairs of divergent arrows can be observed at several points along the fault line itself (Figure 6). The divergent vectors are associated with two grid points split apart by the discontinuity (see Appendix A) and where corresponding displacements are calculated accordingly. The pairs of divergent displacement vectors calculated along the fault trace suggest that relative motions occur at blocks contacts, which are separated by the discontinuity. Significant relative motions (i.e., dextral strike slip) are suggested for the ENE-WSW Møre-Trøndelag Fault Complex in its present state of stress, which is consistent with the applied boundary conditions given in Figure 4. The most important dextral strike-slip displacements affect the central part of the zone of weakness in the area north of the Sogn Graben (Figure 6).

4.3. Simulation of Slip Lineations Along Major Fault Planes Using SORTAN

As the final modeling step, we simulated the sense of slip along preexisting major fault planes belonging to the mid-Norwegian margin and the northern North Sea. As described above, the input parameters are the local stress state (i.e., orientation and shape ratio) and the geometry of the fault plane (see Appendix B). The two geometrical parameters related to each fault plane (e.g., dip and dip direction, Table 1) were taken from previously published seismic lines and structural maps [*Huser*, 1994; *Faerseth et al.*, 1995; *ter Voorde*, 1996; *Faerseth*, 1996; *Christiansson et al.*, 2000]. In cases where depth-converted versions were not available, depth conversion was done by us using available velocity data (e.g., ocean bottom seismometer lines). Stress orientations calculated by UDEC were taken as input for the SORTAN model. In particular, we collected the stress orientations calculated by UDEC in the neighborhood of each fault to determine average σ_H and σ_h strike values. The coherency between calculated stress orientations at each grid point was carefully checked for each collected set. As described above, our 2-D UDEC model is only able to simulate stresses in the horizontal plane. During horizontal shortening, $\sigma_H = \sigma_1$, whereas σ_h can be either σ_3 (strike-slip regime) or σ_2 (reverse regime). Two different SORTAN simulations were performed.

Assuming that the regional stress regime is strike-slip in type, where $\sigma_H = \sigma_1$ striking NW-SE and $\sigma_h = \sigma_3$ (Figure 8, solid curves on stereonets) the following results were obtained. (1) Most of the simulated motions along fault planes are likely to be oblique slip. (2) Although the tectonic stress is compressive, oblique normal faulting can occur (e.g., fault 8). This effect depends both on the orientation of the fault plane as related to the applied stress and on the value of the ratio Φ. High values of Φ (e.g., Φ close or equal to 1, which means σ_1 close or equal to σ_2) favor normal faulting along planes whose strike is close to σ_1 strike. (3) The shape ratio Φ is a very important parameter in defining the sense of slip on faults when those are oblique to the applied stress axes [see also *Wallace*, 1951, Figure 3]. Permutations of shifts from nearly dip-slip to strike-slip faulting can be expected as a function of the shape ratio (see, for example, faults 7, 9, 12, 13, 15 and 17 in Figure 8).

Application of reverse stress regime, where $\sigma_H = \sigma_1$ striking NW-SE and $\sigma_h = \sigma_2$ (Figure 8, shaded curves on stereonets), gives the following results. (1) Reverse dip-slip motions are favorably simulated (see, for example, faults 7, 9, 12, 13, 15, 17, 19, 20, 21, 22, and 24 in Figure 8). (2) In the present case the predicted sense of motion along one given fault is generally less sensitive to the ratio Φ than in the strike-slip case (compare, for example, predicted motions along faults 7, 9, 12, 13, 15, 17, 19, 21, 22, 23, and 24 for strike-slip and for reverse regimes). (3) The simulated motions along the complete set of faults are more consistent in the reverse regime case than in the strike-slip regime one. In particular and despite the obliquity between some fault planes and the main principal stress axis applied (see fault 8 in Figure 8 and Table 1), no normal faulting was simulated for the reverse regime case.

5. Discussion

Stress patterns predicted by UDEC for the mid-Norwegian margin and the northern North Sea (Figure 5) fit with those determined from borehole breakouts, focal mechanisms, and in situ measurements [e.g., *Spann et al.*, 1991; *Fejerskov et al.*, 1995]. The UDEC model duplicates the observed counter-clockwise rotation of the stress field from the mid-Norwegian margin, where σ_1 is generally striking NW-SE to σ_1 striking WNW-ESE as observed in the northern North Sea. In addition, the simulated nearly isotropic stress field in the northern North Sea can explain the complexity and the discrepancies in orientation of the actual stress field [*Lindholm et al.*, 1995]. In the modeled case we expect the

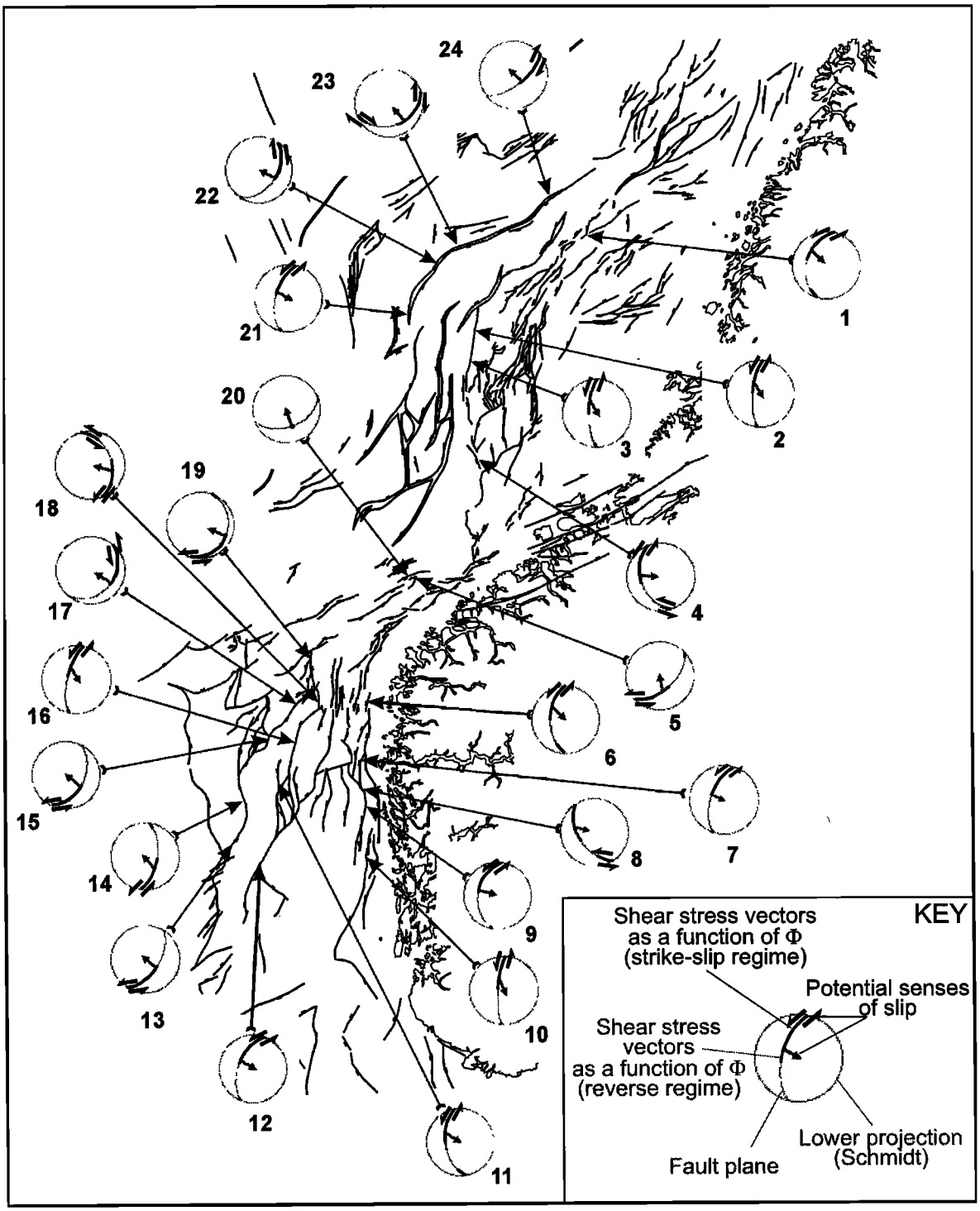

Figure 8. Results of the calibrated modeling UDEC plus SORTAN. Local principal stresses directions are simulated by UDEC (Figure 5 and Table 1). Fault geometries are from various sources (see Table 1). Potential slip directions are given in function of the shape ratio Φ for strike-slip regime (solid curves) and for reverse regime (shaded curves). Intersections between solid and shaded curves correspond to the transitional case between strike-slip and reverse regime (i.e., correspond to Φ=0).

stress field to be very sensitive to local effects (caused by structure, changes in pore pressure, etc). Therefore stress rotations and stress axes permutations would be common.

Our 2-D model cannot account for vertical motions, and it has not been possible to incorporate the effects of the Cenozoic uplift of Scandinavia [e.g., *Doré*, 1992; *Rohrmann et al.*, 1995, 1996; *Rohrmann and van der Beek*, 1996; *Gudmundsson*, 1999]. Neither is it possible to take into account topographic effects, which might be locally important close to the elevated Scandinavian shield.

Still, our model is in good agreement with the present-day stress field [*Fejerskov et al.*, 1995], which reveals that NNW-SSE reorientation of the major principal stress axis occurs inside the zone of weakness associated with the Møre-Trøndelag Fault Complex. Despite the limited amount of offshore data along the fault zone itself one can observe a good consistency in stress axes orientation.

The present models suggest that contrasting stress patterns between north and south of the Møre-Trøndelag Fault Complex exist. Similar effects are observed for other crustal-scale dislocations like the San Adreas Fault [*Zoback et al.*, 1987; *Zoback*, 1991] and West Spitsbergen [*Maher and Craddock*, 1988]. We emphasize the influence on stress trajectories of less competent rocks located inside the fault zone (e.g., the weak zone). Although our choice of introducing an elastic rheology to simulate the behavior of the weak zone seems too simplistic (plasticity laws rather than Hooke's law would be more accurate to restore natural deformation in such a context), two points merit discussion.

First, the Young's modulus of the weak zone associated with the zone of weakness was set to 3 GPa in the present simulation (Figure 4). *Walsh* [1965] demonstrated analytically that rocks affected by elliptic cracks are characterized by lower Young's modulus values compared to the corresponding intact rocks. Laboratory experiments applying shock-damaged rocks [*Hogliang and Ahrens*, 1994] showed that these rocks display Young's modulus values of 1-2 orders of magnitude less than those measured applying intact rocks, in agreement with the analytical result of *Walsh* [1965]. Although it is questionable to which degree the properties of natural fractures, which are potentially affected by healing and sealing, can be compared to simple elliptic cracks, it is interesting to note that we need to drop the Young's modulus value of the fault zone in our model ~1 order of magnitude to obtain significant effects (Figure 7). Thus our quantitative analysis agrees with the experimental results from *Hogliang and Ahrens* [1994]. On the other hand, what is considered to be a weak zone in our model is, in fact, a complex zone of deformation, where small-scale fault blocks and basement fault blocks are included in the zone. Because high fracture frequencies are restricted to volumes close to the major faults, additional mechanisms (e.g., shallowing of the brittle-ductile transition inside the fault zone [*Stewart et al.*, 2000]) to those proposed by *Walsh* [1965] must contribute to the fault zone weakening.

Second, the present 2-D model is only valid for the brittle domain of the upper crustal levels. If our assumption on the shield effect of the zone of weakness is correct, it should be expected that the fault zone affects the whole lithosphere and that mechanical weakening of the fault zone also occurs in the lower crust and possibly in the upper mantle. On the basis of deep seismic lines, *Hurich and Kristoffersen* [1988] and *Hurich* [1996] suggested a lithospheric nature for the Møre-Trøndelag Fault Complex. The long-lasting activity of the fault complex strongly suggests that it is a major zone of weakness with probably deep roots. Moreover, additional geophysical data (gravimetry (see Figure 2) and magnetic data [*Doré et al.*, 1997]) also suggest deep roots.

Another matter of discussion is the origin and the consistency in time of the stresses applied to the studied domain. For our modeling we inferred that the Atlantic ridge push is the unique source of stresses since earliest Eocene to present day.

The question is addressed by *Vågnes et al.* [1998]. These authors observed that the Ormen Lange Dome in the mid-Norwegian margin has been growing continuously with a very striking constant rate since earliest Eocene [see *Vågnes et al.*, 1998, Figure 4, p. 37]; similar results are reported for the Helland-Hansen Arch [*Langaker*, 1998]. These data suggest surprisingly that no major changes occurred in the direction of compression, nor in the magnitudes of far-field stresses. Furthermore, minor changes (e.g., < 15°) in the direction of compression at our model boundaries imply minor changes in the simulated stress pattern inside the modeled domain. In contrast, differential loading has been proposed as the main mechanism for the growth of the domes [*Stuevold et al.*, 1992]. However, the widespread occurrence of Cenozoic compressive structures (i.e., NW Scotland [*Geoffroy et al.*, 1994], Faeroe Plateau [*Boldreel and Andersen*, 1998], and east Greenland (D. Strogen, personal communication, 2000)) favors our hypotheses.

Influence of alpine events on the studied area are deemed minor for two reasons. First, it is difficult to explain in the present context compressive structures induced by alpine stresses (hence transmitted from the south) along the margin, whereas the northern North Sea remains relatively quiet. Second, present-day measurements show stress directions consistent with the Alpine compression (NW-SE) in the southern North Sea [*Müller et al.*, 1992], whereas stress directions measured in the northern North Sea are inconsistent with the general strike of alpine forces. However, alpine stresses in the northern North Sea are also deflected and not strictly unefficient. Also, other lithospheric-scale lineaments (e.g., the Hardangerfjord-Ling Graben-Highland Boundary Fault [*Jones and Geoff Tramer*, 1995]) can induce similar effects as the Møre-Trøndelag Fault Complex.

Our last modeling experiment was to reconstruct the senses of potential slip along major fault planes (Figure 8). The reconstruction was made using local stress states simulated by UDEC as input for SORTAN. We present this effort as direction for future developments rather than an improved model. The major problem in the modeling is to "jump" from a 2-D model (i.e., UDEC) to a 3-D model (i.e., SORTAN), that is to say, to determine the 3-D configuration of the principal stress axes. The two possible compressive stress regimes (i.e., strike slip and reverse) are considered in the SORTAN modeling.

Existing evidence from earthquake focal mechanisms from the sedimentary basins offshore mid-Norway demonstrate that normal movements on faults are subordinate to strike-slip and reverse movement. This is consistent with the assumed present NW-SE directed compressional stress field.

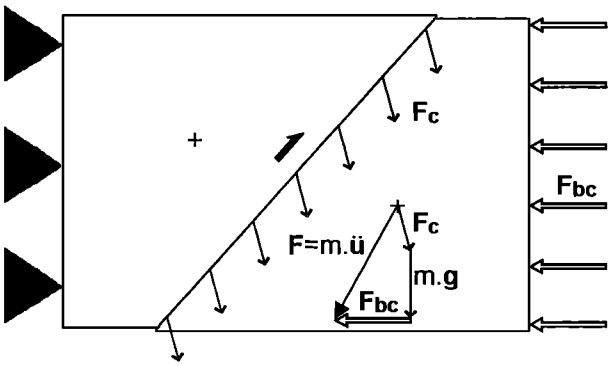

Figure A1. Distinct element method: example of out of balance forces applied to the centre of gravity of one block. $\mathbf{F_{bc}}$, force arising from boundaries conditions; $\mathbf{F_c}$, contact force; m.**g**, gravitational force; **F**, vectorial sum of forces; m, block mass; **ü**, acceleration of the center of gravity of the block.

Furthermore, we find that these results are in better harmony with the strike-slip regime model, where $\sigma_1=\sigma_H=\sigma_{NW\text{-}SE}$, $\sigma_2=\sigma_v$, and $\sigma_3=\sigma_h=\sigma_{NE\text{-}SW}$. Indeed, paleostress analysis [e.g., *Bergerat*, 1987] suggests that strike-slip faulting is common in contractional regimes, where the source of the compression is situated far away from the studied area. This is in concert with the assumption that ridge push is the main source for the Cenozoic stress in the study area. In addition, our assumption is justified from a mechanical point of view in considering the rock loading, which would easily produce permutations between σ_2 and σ_3 and therefore favor strike-slip regimes in compressive contexts.

6. Conclusions

Two modeling tools have been used in the present study. First, we reconstructed present-day stress and displacement patterns using the 2-D distinct element method (UDEC). The results are assumed to be valid first-order patterns from earliest Eocene (i.e., from continental breakup) to present day.

We show how the Møre-Trøndelag Fault Complex and its continuation into the Shetland Platform may act as a shield, protecting the northern North Sea from Atlantic ridge push forces. In this model, maximum displacement vectors are mainly focused along the margin, where Cenozoic compressional structures are commonly recognized. Mechanical weakening of the fault zone is suggested at the lithospheric scale. Thus introducing the Møre-Trøndelag Fault Complex and its continuation as a weak zone in our model allows us to restore observed present-day stress patterns inside the northern North Sea and inside the mid-Norwegian margin.

Second, we used SORTAN in combination with UDEC to restore senses of potential motions along major fault planes. We showed, following *Wallace* [1951], the importance of the degree of anisotropy of the applied stress state (e.g., the value of the shape ratio Φ) in leading the sense of motion along faults. Again, because it is a function of various parameters (tectonic in-plane forces, depth, and local discrepancies), the ratio Φ is very difficult to determine. Nevertheless, more local studies can provide constraints on the stress state near the major fault planes of the northern North Sea and the mid-Norwegian margin. Also, more accurate predictions on the senses of slip can be done.

Appendix A: Principles of the Distinct Element Method

A1. Calculation of Block Displacements

Block displacements are calculated from out of balance moment and forces applied to the center of gravity of each block (Figure A1). Resultant forces (labeled F in (A1)) include boundary forces applied to the edges of the block and, eventually, gravity when introduced by the user.

Newton's second law is applied for each block:

$$\frac{\partial \dot{\mathbf{u}}(t)}{\partial t} = \frac{\mathbf{F}(t)}{m}, \tag{A1}$$

where $\dot{\mathbf{u}}$ is velocity, m is mass, and t is time.

Following finite differences techniques, (A1) can be transformed into

$$\dot{\mathbf{u}}(t+\Delta t/2) = \dot{\mathbf{u}}(t-\Delta t/2) + \frac{\mathbf{F}(t)}{m}\Delta t\,. \tag{A2}$$

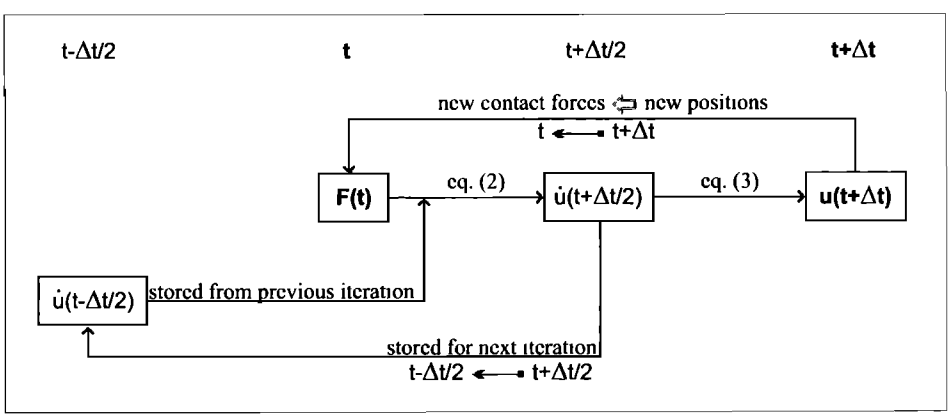

Figure A2. Basic calculation scheme for the distinct element method. See Appendix A for details.

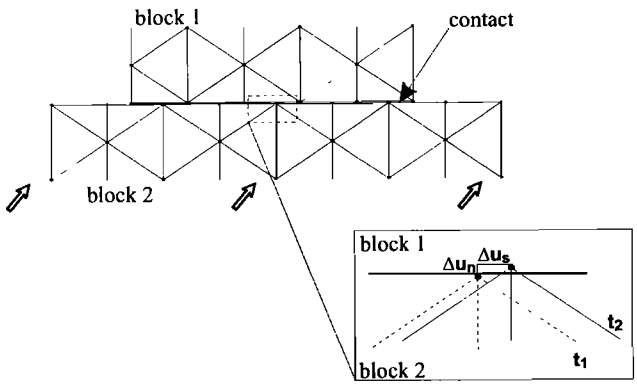

Figure A3. Determination of relative motions of blocks 1 and 2 at their contact. Increments in normal displacements Δu_n and shear displacements Δu_s are calculated between time t_1 and time t_2 at each block boundary grid points.

Storing velocities at each half time step point (Figure A2) allows calculation of displacements:

$$\mathbf{u}(t+\Delta t) = \mathbf{u}(t) + \dot{\mathbf{u}}(t+\Delta t/2)\Delta t\,. \tag{A3}$$

The new position of the block induces new conditions at block boundaries and thus new contact forces. The calculation scheme summarized above by (A1)-(A3) is repeated until equilibrium is reached for each block (Figure A2). Angular velocities and displacements are involved in the same fashion in the calculation scheme [see *Last and Harper*, 1990].

A2. Constitutive Laws of Contacts and Block Interactions

Out of balance forces and moments applied to the centers of gravity of the blocks arise partially from forces applied to their contacts. The constitutive laws applied to the contacts are

$$\Delta\sigma_n = k_n\,\Delta u_n, \tag{A4}$$

$$\Delta\sigma_s = k_s\,\Delta u_s, \tag{A5}$$

where k_n and k_s are the normal and shear stiffness of the contact, $\Delta\sigma_n$ and $\Delta\sigma_s$ and Δu_n and Δu_s are the normal and shear stress increments and the normal and shear displacement increments, respectively (Figure A3).

Finally, stresses calculated at grid points located along contacts (Figure A3) are submitted to the selected yield criterion:

$$|\tau| \le \mu\sigma_n + c_0, \tag{A6}$$

where μ is the coefficient of friction and c_0 is the cohesion. In addition, no tension is permitted along contacts, and hence an additional constraint is added:

$$\sigma_n \ge 0. \tag{A7}$$

A3. Internal Deformation of Blocks

According to the selected constitutive law, internal deformation of blocks can be taken into account in the calculations. Hence mechanical equations are solved meshing the blocks into triangular zones of finite differences (see Figure 3). Newton's second law is then applied at each grid point. Thereafter, the finite differences technique is used again to calculate velocity and strain at each grid point.

The selected constitutive law for the blocks is used to determine stresses at each grid point. For the present study we applied pure elastic conditions as defined by Hooke's Law. Therefore stress and strain are linked at each grid point by

$$\sigma_{ij} = \frac{E}{1+\nu}\varepsilon_{ij} + \frac{E\nu}{(1+\nu)(1-2\nu)}\varepsilon_{kk}\delta_{ij}, \tag{A8}$$

where E is the Young's modulus and ν the Poisson's ratio.

Appendix B: Principles of the SORTAN Method

For the sake of simplicity the SORTAN method is described in function of the ratio Φ introduced by *Angelier* [1975]. A more detailed mathematical description is given by *Pascal* [1998] and *Pascal and Angelier* (hereinafter cited as C. Pascal and J. Angelier, submitted manuscript, 2001).

Consider the applied stress tensor to the fault plane (Figure B1a), where $\sigma_1 \ge \sigma_2 \ge \sigma_3$ and where compression is considered positive. According to *Angelier* [1979], the corresponding stress tensor written in the system of its principal axes T_0 can be reduced into

$$T_R = \begin{pmatrix} 1 & 0 & 0 \\ 0 & \Phi & 0 \\ 0 & 0 & 0 \end{pmatrix}, \tag{B1}$$

with

$$\Phi = (\sigma_2-\sigma_3)/(\sigma_1-\sigma_3), \tag{B2}$$

$$\Phi \in [0;1]. \tag{B3}$$

This technique decreases the number of unknowns related to the 3-D stress tensor from six to four. The four remaining unknowns are three angles which account for the orientation of the three principal stress axes and one dimensionless value, namely, the shape ratio that describes the geometry of the shape of the stress ellipsoid (Figure B1b). Physically, the ratio Φ represents the degree of anisotropy of the applied stress state in the 3-D space (e.g., for $\Phi = 0$ the stress ellipsoid is prolate-shaped and the stress is isotropic in the σ_2-σ_3 plane and for $\Phi = 1$ the stress ellipsoid is oblate-shaped and the stress is isotropic in the σ_2-σ_1 plane; see Figure B1b). Depending on the value of Φ, the slip direction along one given fault will be principally controlled by the fault plane orientation or by the orientation of the stress axes.

Stress tensor reduction implies that all information on the stress magnitudes is lost. However, it has been demonstrated [*Carey and Brunier*, 1974; *Angelier*, 1975] that the information on the orientation of the principal stresses and especially on the orientation of the shear stress vector (i.e., of the slip vector) is kept.

Following *Anderson* [1905, 1951] we add one vertical principal stress axis to the list of assumptions. The latter assumption is another simplification of the analytical

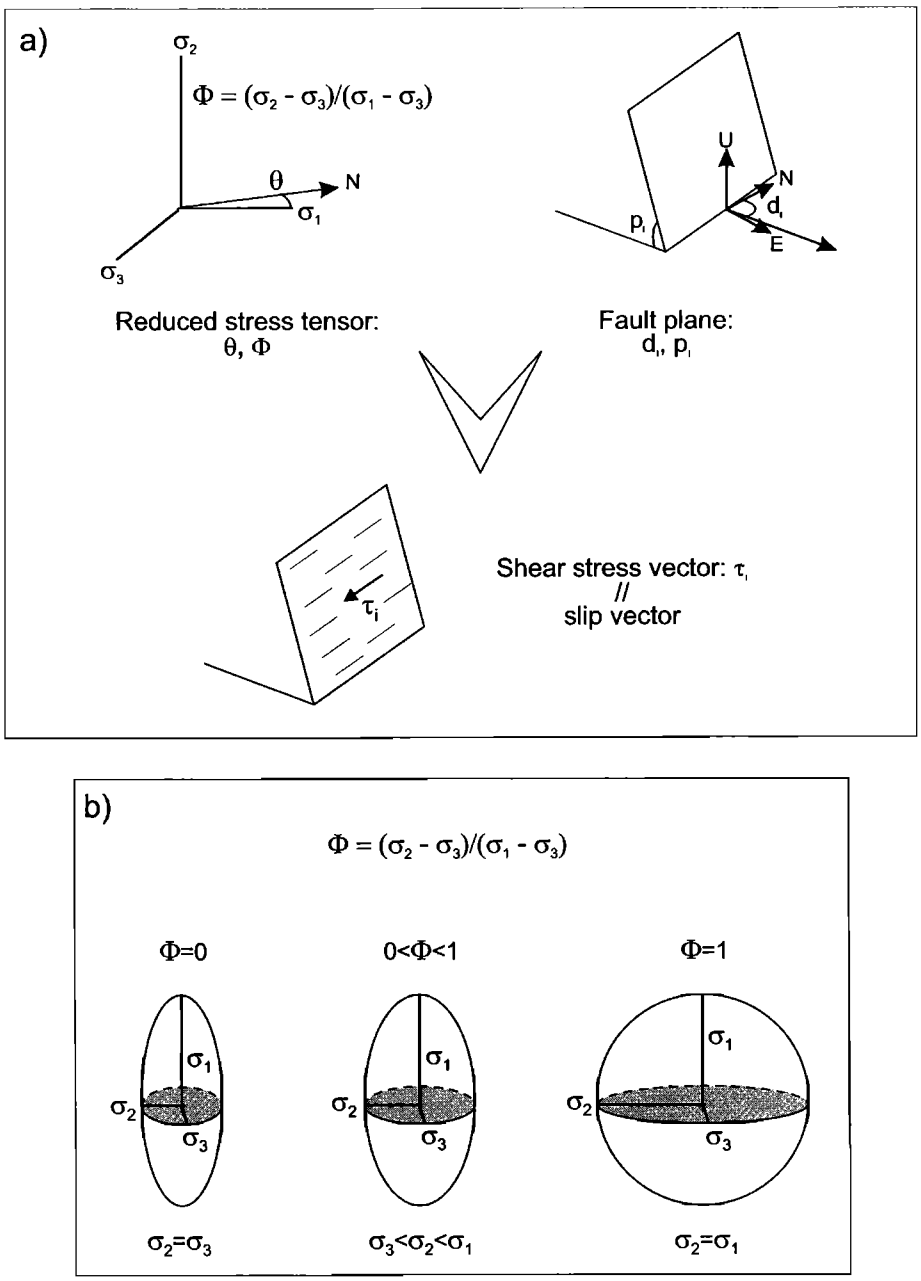

Figure B1. Basic principles of the simplified method SORTAN. (a) Example of determination of the sense of slip along one fault plane induced by a compressive strike-slip stress regime. Two parameters define the reduced stress tensor which is applied: the azimuth of σ_1 (in the present case), θ, and the shape ratio Φ. Two other parameters give the geometrical attitude of the fault plane: the dip direction d_i and the dip p_i. The Cartesian system (E, N, U) corresponds to three unit vectors striking eastward, northward, and upward, respectively. (b) Physical meaning of the shape ratio Φ. For Φ=0 the shape of the stress ellipsoid is prolate; for Φ=1 the shape of the stress ellipsoid is oblate; for $0< \Phi <1$ the geometry of the stress ellipsoid is in between, and the stress state is pure triaxial.

problem. If we know the type of paleostress regime which affected the study area (e.g., pure normal with σ_1 vertical, strike slip with σ_2 vertical, or reverse with σ_3 vertical), the orientations of the three principal axes are determined from the azimuth θ (of one of the two horizontal principal axes, Figure B1a). Therefore, when the stress regime is known, only two parameters are needed to characterize the applied reduced stress tensor: the ratio Φ and the azimuth θ.

The stress tensor is written according to the selected Cartesian system and applied to one given fault plane defined

by its dip direction d and its dip p (Figure B1a). Finally, the shear stress vector is calculated and written as a function of Φ, θ, d and p.

Acknowledgments. The authors would like to thank Sintef Petroleum Research, Norsk Hydro ASA, Mobil, the Research Council of Norway, and the Geological Survey of Norway for their interest in this work and financial support and Kuvvet Atakan and Walter Wheeler for fruitful discussions. Olav Eldholm, August Gumundson, and Tim Redfield are acknowledged for critical and useful comments on an early version of the paper. Eric Barrier is particularly thanked for improving the paper by his very helpful review. We are grateful to Michel Heeremans for his help in providing the gravity anomaly map. Part of the modeling work was carried out at Laboratory of Tectonophysics, University of Paris VI

References

Aanstad, K.M., R.H., Gabrielsen, T., Hagevang, I.B., Ramberg, and O., Torvanger, Correlation of offshore and onshore structural features between 62°N and 68°N, Norway, in *Proceedings, Norwegian Symposium on Exploration, Bergen 1981, NSE/11*, pp. 1-24, Nor. Petrol. Soc., Stavanger, 1981.

Anderson, E.M., The dynamics of faulting, *Trans Edinburgh Geol. Soc.*, 8 (3), 393, 1905.

Anderson, E.M., *The Dynamics of Faulting and Dyke Formation With Applications to Britain*, 2nd ed., 206 pp., Oliver and Boyd, White Plains, N.Y., 1951.

Angelier, J., Sur l'analyse de mesures recueillies dans des sites faillés: L'utilité d'une confrontation entre les méthodes dynamique et cinématique, *C.R. Acad. Sci., 281*, 1805-1808, 1975 (Erratum *C.R Acad. Sci., 283*, 466, 1976).

Angelier, J., Determination of the mean principal directions of stresses for a given fault population, *Tectonophysics, 56*, 17-26, 1979.

Bergerat, F., Stress fields in the European platform at the time of Africa-Eurasia collision, *Tectonics, 6*, 99-132, 1987.

Blystad, P., H., Brekke, R.B., Faerseth, B.T., Larsen, J., Skogseid, and B.,Torudbakken, Structural Elements of the Norwegian Continental Shelf, Part II, The Norwegian Sea Region, *Bull. Nor. Petrol. Soc., 8*, 45 pp., 1995.

Boldreel, L.O., and M.S, Andersen, Tertiary compressional structures on the Faeroe-Rockall Plateau in relation to northeast Atlantic ridge-push and Alpine foreland stresses, *Tectonophysics, 300*, 13-28, 1998.

Bott, M.H.P., The mechanics of oblique slip faulting, *Geol. Mag , 96*, 109-117, 1959.

Bungum, H., A., Alsaker, L.B , Kvamme, and R.A., Hansen, Seismicity and seismotectonics of Norway and nearby continental shelf areas, *J. Geophys. Res, 96*, 2249-2265, 1991.

Byerlee, J.D., Friction of rocks, *Pure Appl. Geophys., 116*, 615-626, 1978.

Byrkjeland, U., H., Bungum, and O., Eldholm, Seismotectonics of the Norwegian continental margin, *J. Geophys. Res, 105*, 6221-6236, 2000.

Carey, E., and B., Brunier, Analyse théorique et numérique d'un modèle mécanique élémentaire appliqué à l'étude d'une population de failles, *C.R. Acad. Sci., 279*, 891-894, 1974

Carmichael, R.S., *Practical Handbook of Physical Properties of Rocks and Minerals*, CRC Press, Boca Raton, Fla., 1989.

Christiansson, P , J.I., Faleide, and A.M., Berge, Crustal structure in the northern North Sea, an integrated geophysical study, in *Dynamics of the Norwegian Margin*, edited by A Nøttvedt, pp. 15-40, Spec. Pub. Geol. Soc. London, 167, 2000.

Cundall, P.A , A computer model for simulating progressive large scale movement in blocky rock systems, in *International Symposium on Rock Mechanics*, Ecole Nati. Supérieure de Géol. Appliquée et de Prospection Minière, Nancy, France, 1971.

Cundall, P.A., UDEC, a generalised distinct element program for modeling jointed rock, *Contract Rep. DAJA 37-39-C-0548, U.S. Army Eur. Res. Office and Defence Nucl. Agency*, London, 1980.

Doré, A G., The base tertiary surface of southern Norway and the northern North Sea, *Nor. Geol. Tidssk., 72*, 259-265, 1992.

Doré, A.G., and M.S., Gage, Crustal alignments and sedimentary domains in the evolution of the North Sea, north-east Atlantic margin and barents shelf, in *Petroleum Geology of North West Europe*, edited by J. Brooks and K. Glennie, pp. 1131-1148, Graham and Trotman, Boston, Mass., 1987.

Doré, A.G., and E.R., Lundin, Cenozoic compressional structures on the NE Atlantic margin: Nature, origin and potential significance for hydrocarbon exploration, *Petrol Geosci., 2*, 299-311, 1996.

Doré, A.G., E R., Lundin, C. Fichler, and O., Olesen, Patterns of basement structure and reactivation along the NE Atlantic margin, *J Geol. Soc London, 154*, 85-92, 1997.

Eldholm, O., A.M., Karasik, and P.A., Reksnes, Geology of the Arctic Ocean region: Recent results and outstanding problems, in *The Geology of North America, vol. IL, The North America Plate Boundary*, edited by A. Grantz, G.L. Johnson and J. Sweeny, pp. 171-184, Geol. Soc. of Am., Boulder, Colo., 1990.

Faerseth, R.B., Interaction of Permo-Triassic and Jurassic extensional fault-blocks during the development of the northern North Sea, *J. Geol. Soc. London, 153*, 931-944, 1996.

Faerseth, R.B., R.H., Gabrielsen, and Hurich, C.A., Influence of basement in structuring of the North Sea Basin, offshore southwest Norway, *Nor. Geol. Tidssk., 75*, 105-119, 1995.

Fejerskov, M., A.M., Myrvang, C., Lindholm, and H., Bungum, In-situ rock stress pattern of the Norwegian continental shelf and mainland, in *Proceedings of the Workshop on Rock Stresses in the North Sea, Trondheim, Norway, 13-14 February 1995*, edited by M. Fejerskov and A.M. Myrvang, pp. 191-201, SINTEF, Rock and Min. Eng., Trondheim, Norway, 1995.

Gabrielsen, R.H., Reactivation of faults on the Norwegian Continental Shelf and its application for earthquake occurrence, in *Earthquakes at North-Atlantic Passive Margins: Neotectonics and Postglacial Rebound*, edited by S. Gregersen and P.W. Basham, pp. 67-90, Kluwer Acad., Norwell, Mass., 1989.

Gabrielsen, R.H., and I.B., Ramberg, Fracture patterns in Norway from Landsat imagery. Results and potential use, *Proceedings, Norwegian Sea Symposium, Tromsø 1979, NSP/1-28*, Nor. Petrol. Soc., Stavanger, 1979.

Gabrielsen, R.H., R., Færseth, G., Hamar, and H., Rønnevik, Nomenclature of the main structural features on the Norwegian continental shelf north of the 62nd parallel, in *Petroleum Geology of the North European Margin*, edited by A.M. Spencer et al., pp. 41-60, Graham and Trotman, London, 1984.

Gabrielsen, R.H., T., Odinsen, and I., Grunnaleite, Structuring of the northern Viking Graben and the Møre Basin: The influence of basement structural grain, and the particular role of the Møre-Trøndelag Fault Complex, *Mar. Petrol. Geol., 16*, 443-465, 1999.

Geoffroy, L., F., Bergerat, and J., Angelier, Tectonic evolution of the Greenland-Scotland ridge during the Paleogene: New constraints, *Geology, 22*, 653-656, 1994.

Golke, M., S., Cloetingh, and D., Coblentz, Finite-element modeling of stress patterns along the Mid-Norwegian continental margin, 62° to 68°N, *Tectonophysics, 266*, 33-53, 1996

Grunnaleite, I, and R.H., Gabrielsen, Structure of the Møre Basin, mid-Norway continental margin, *Tectonophysics, 252*, 221-251, 1995

Grønlie, A. and D., Roberts, Resurgent strike-slip duplex development along the Hitra-Snasa and Verran Faults, Møre-Trøndelag Fault Zone, central Norway, *J. Struct. Geol., 11*, 295-305, 1989.

Grønlie A., V., Harder, and D., Roberts, Preliminary fission-track ages on fluorite mineralisation along fracture zones, inner Trondheimsfjord, Central Norway, *Nor. Geol. Tidssk , 70*, 173-178, 1990.

Gudmundsson, A., Postglacial crustal doming, stresses and fracture formation with application to Norway, *Tectonophysics, 307*, 407-419, 1999.

Hogliang, H. and T.J., Ahrens, Mechanical properties of shock-damaged rocks, *Int. J. Rock Mech. Min. Sci. Geomech. Abstracts, 31*, 525-533, 1994.

Homberg, C., J.C., Hu, J., Angelier, F., Bergerat and O., Lacombe, Characterization of stress perturbations near major fault zones: Insights from 2-D distinct-element numerical modeling and field studies (Jura Mountains), *J. Struct. Geol., 19*, 703-718, 1997

Hurich, C.A., Kinematic evolution of the lower plate during intracontinental subduction: An example from the Scandinavian Caledonides, *Tectonics, 15*, 1248-1263, 1996.

Hurich, C.A., and Y., Kristoffersen, Deep structure of the Caledonide orogen in southern Norway New evidence from marine seismic reflection profiling, *Spec. Pub Nor. Geol. Undersøkelse, 3*, 66-69, 1988.

Huser, E., *En vurdering av rekonstruksjonsprogrammet Echo-Pal basert på geologiske data from Oseberg området (Blokk 30/9, nordlige Nordsjø)*, candidate sci. thesis, Univ. of Oslo, Oslo, 1994.

Jones, R.R., and P.W., Geoff Tramer, Strain partitioning in transpression zones, *J. Struct. Geol., 17*, 793-802, 1995.

Jordt, H., J.I., Faleide, K., Bjørlykke, and M T., Ibrahim, Cenozoic sequence stratigraphy of the central northern North Sea Basin: Tectonic development, sediment distribution and provenance areas, *Mar. Petrol. Geol., 12*, 845-879, 1995.

Kjennerud, T., *Structural restoration of palaeobathymetry during the Creataceous in the northern North Sea*, diploma thesis, Dep. of Geol. and Miner. Resour. Eng., Nor. Univ. of Sci. and Technol., Trondheim, Norway, 1997.

Langaker, K., *Strukturell utvikling av Helland-Hansenhvelvet, Vøringbassenget, gjennom tertiær tid* (Structural development of the Helland Hansen Arch, the Vøring Basin, throughout the Tertiary), candidate sci. thesis, Univ. of Bergen, Bergen, Norway, 1998.

Last, N.C., and T.R., Harper, Reponse of fractured rock subject to fluid injection, part I, Development of a numerical model, *Tectonophysics, 172*, 1-31. 1990.

Lindholm, C., H., Bungum, M., Villagran, and E., Hicks, Crustal stress and tectonics in Norwegian regions determined from

earthquake focal mechanisms, in *Proceedings of the Workshop on Rock Stresses in the North Sea, Trondheim, Norway, 13-14 February 1995*, edited by M. Fejerskov and A M Myrvang, pp 77-91, SINTEF, Rock and Min Eng., Trondheim, Norway, 1995.

Maher, H.D., Jr, and C.L., Craddock, Decoupling as an alternate model for transpression during the initial opening of the Norwegian-Greenland Sea, *Polar Res.*, 6, 137-140, 1988.

Midzi, V., D.D., Singh, K, Atakan, and J., Havskov, Transitional continental-oceanic structure beneath the Norwegian Sea from inversion of surface wave group velocity data, *Geophy. J. Int.*, *139*, 433-446, 1999.

Müller, B , M.L., Zoback, K., Fucks, L., Mastin, S., Gregersen, N., Pavoni, O., Stephansson, and C , Ljunggren, Regional patterns of tectonic stress in Europe, *J. Geophys Res.*, *97*, 11,783-11,803, 1992.

Oftedahl, C., A sideretic ironstone of Jurassic age in Beistadfjorden, Trøndelag, *Nor. Geol Tidssk.*, *52*, 123-134, 1972.

Oftedahl, C., Middle Jurassic graben tectonics in mid-Norway, in *Proceedings from Jurassic Northern North Sea symposium*, Norwegian Petroleum Society, 21pp., 1975.

Pascal, C., *Etude mécanique et modélisation de la fracturation en extension, application au domaine de la Mer du Nord*, thèse de doctorat, Sci de la Terre, Univ P M. Curie, Paris, 1998.

Price, I., and R.P., Rattey, Cretaceous tectonics off mid-Norway: Implications for the Rockall and Faeroe-Shetland troughs, *J Geol. Soc. London*, *141*, 985-992. 1984.

Rohrman, M., and P. A , van der Beek, Cenozoic domal uplift of North Atlantic margins: An asthenospheric diapirism model, *Geology*, *24*, 901-904, 1996.

Rohrman, M., P.A., van der Beek, P.A.M., Andriessen, and S., Cloetingh, Meso-Cenozoic morphotectonic evolution of southern Norway: Neogene domal uplift inferred from apatite fission track thermochronology, *Tectonics*, *14*, 704-718, 1995.

Rohrman, M., P., Andriessen, and P.A., van der Beek, The relationship between basin and margin thermal evolution assessed by fission track thermochronology· An application to offshore southern Norway, *Basin Res.*, *8*, 45-63, 1996.

Sandwell, D.T., and W H F., Smith, Marine gravity anomaly from Geosat and ERS-1 altimetry, *J Geophys. Res.*, *102*, 10,039-10,054, 1997.

Séranne, M., Devonian extensional tectonics versus Carboniferous inversion in the northern Orcadian basin, *J. Geol Soc London. 149*, 27-37, 1992.

Spann, H., M , Brudy, and K., Fuchs, Stress evaluation in offshore regions of Norway, *Terra Nova*, *3*, 148-152, 1991.

Stewart, M., R.E., Holdsworth, and R.A., Strachan, Deformation processes and weakening mechanisms whithin the frictional-viscous transition zone of major crustal-scale faults. Insights from the Great Glen Fault Zone, Scotland, *J. Struct. Geol.*, *22*, 543-560, 2000.

Stuevold, L.M., J., Skogseid, and O., Eldholm, Post-Cretaceous uplift events on the Voring continental margin, *Geology*, *20*, 919-922, 1992.

Sykes, L.R., The seismicity of the Arctic, *Seismol. Soc. Am. Bull*, *55*, 501-518, 1965.

Talwani, M., and O., Eldholm, The continental margin off Norway: A geophysical study, *Geol. Soc. Am Bull.*, *83*, 3375-3608, 1972.

Talwani, M., and O., Eldholm, Evolution of the Norwegian-Greenland Sea, *Geol. Soc Am. Bull.*, *88*, 969-999, 1977.

ter Voorde, M., *Tectonic modeling of lithospheric extension along fauts; implications for thermal and mechanical structure and basin stratigraphy*, PhD thesis Vrije Univ., Amsterdam, 1996.

Torsvik, T.H., B.A., Sturt, D.M., Ramsay, A., Grønlie, D., Roberts, M., Smethurst, K., Atakan, R., Bøe, and H.J., Walderhaug, Palaeomagnetic constraints on the early history of the Møre-Trøndelag Fault Zone, Central Norway, in *Palaeomagnetic Rotations and Continental Deformation*, edited by. C Kissel and C. Laj, pp 431-457, Kluwer Acad., Norwell, Mass., 1989.

Stephansson, O , Ridge push and glacial rebound as rock stress generators in Fennoscandia, *Bull Geol Instit. Univ. Uppvala*, *14*, 39-48, 1988.

Vågnes, E., R.H., Gabrielsen, and P , Haremo, Late Cretaceous-Cenozoic intraplate contractional deformation at the Norwegian continental shelf, timing, magnitude and regional implications, *Tectonophysics*, *300*, 29-46, 1998.

Wallace, R.E., Geometry of shearing stress and relation to faulting, *J. Geol.*, *59*, 118-130, 1951

Walsh, J.B., The effect of cracks on the uniaxial elastic compression of rocks, *J Geophys. Res*, *70*, 399-411, 1965.

Ziegler, P.A., *Geological Atlas of Western and Central Europe 2nd ed*, 239 pp., Shell Int Petrol Maatschappij B V., The Hague, The Netherlands, 1990

Zoback, M.D., State of stress and crustal deformation along weak transform faults, *Philos. Trans. R Soc London, Ser A*, *337*, 141-150, 1991

Zoback, M D., et al., New evidence on the state of stress of San Andreas fault system, *Science*, *238*, 1105-1111, 1987.

C. Pascal, Faculty of Earth Sciences, Vrije Universiteit, De Boelelaan 1085, 1081 HV Amsterdam, Netherlands. (pasc@geo vu.nl)

R. H. Gabrielsen, Geological Institute, University of Bergen, Allégaten 41, N-5007 Bergen, Norway. (roy.gabrielsen@geol.uib.no)

(Received May 11, 2000;
revised February 5, 2001,
accepted February 9, 2001.)